Desalination and Water Treatment
www.deswater.com

22 (2010) 133–145
October

doi: 10/5004/dwt.2010.1658

Microfiltration of stable oil-in-water emulsions using kaolin based ceramic membrane and evaluation of fouling mechanism

B.K. Nandi, R. Uppaluri, M.K. Purkait*

Department of Chemical Engineering, Indian Institute of Technology, Guwahati 781039, Assam, India
Tel. +91 3612582260/2582262*; email: mihir@iitg.ernet.in*

Received 26 November 2009; Accepted 26 April 2010

ABSTRACT

This work addresses experimental and modeling studies on the treatment of oily wastewater emulsions using prepared lowcost ceramic membrane. Flat circular disk type membranes (52.5 mm diameter and 4.5 mm thickness) were used for microfiltration (MF) tests possessed a hydraulic pore diameter of 0.77 μm and total porosity of 42%. Synthetic oil-in-water emulsions constituting 50–150 mg/l oil concentrations were subjected to MF in batch mode of operation with varying transmembrane pressure differentials (ΔP) ranging from 41.37 to 206.8 kPa. Typical permeate flux of 15.05×10^{-6} m^3/m^2 s and a rejection efficiency of 98.51% was observed for 150 mg/l feed oil concentration at ΔP of 206.8 kPa. Different pore blocking models such as complete pore blocking, standard pore blocking, intermediate pore blocking and cake filtration were used to gain insights into the nature of membrane fouling during permeation. The observed flux decline data trends infer that the decrease in permeate flux is due to intermediate pore blocking for the initial 1–10 min and later by cake filtration. Linear extrapolation of the data trends reveals that for feed oil concentrations above 250 mg/l, only cake filtration would be the flux decline mechanism. Finally, phenomenological models were proposed to illustrate the dependency of total hydraulic resistance of membrane on ΔP, initial oil concentration (c) and time (t).

Keywords: Microfiltration; Ceramic membrane; Oil-in-water; Flux decline; Cake filtration

1. Introduction

Various process industries such as petroleum refineries, petrochemical industries, metallurgical, transportation and food processing industries produce large volumes of oily wastewater. Typical composition ranges of produced oil-in-water (o/w) emulsions vary between 50 and 1000 mg/l of total oil and grease and 50–350 mg/l of total suspended solids [1]. Existing tolerance limits of total oil and grease concentrations in wastewater streams is about 10–15 mg/l [1]. To achieve the desired discharge limits, conventional processes such as thermal de-emulsification [2], electroflotation [3], biological methods [4], coagulation [5] and chemical treatment methods [6] are effective for the treatment of o/w waste streams with high feed concentrations (500–5000 mg/l). On the other hand, due to the existence of smaller droplet sizes (<1 μm) of the emulsions for lower feed concentrations (50–500 mg/l) these methods are ineffective for the removal of oil [7]. Amongst various alternative technologies plausible for such applications, membrane technology is promising due to various advantages such as lower capital cost, higher separation factors, compact design and the elimination of other chemical and mechanical treatment units such as mechanical

*Corresponding author.

separation, electroflotation, filtration and chemical de-emulsification [8].

To date, several articles have been published illustrating the excellent potential of polymeric membranes and ceramic membranes [8–11] for the treatment of o/w emulsions. Though inexpensive with a reported cost of 50–200 $/m^2 [12] during filtration, polymeric membranes are susceptible to fouling and degradation and eventually needs to be replaced frequently. As a result operating cost increases significantly [10]. In addition, each polymeric membrane has its own solvent compatibility and weakness to specific chemicals present in the permeating liquid. For instance, cellulose acetate membranes are severely affected by the presence of chlorine and solvents such as acetone and aniline [12].

On the other hand, due to their inherent chemical, thermal and mechanical stability, zirconia and alumina [11] based ceramic membranes are less prone to fouling. As a result, ceramic membranes offers longer life span of 3–5 years and are found to be promising for the treatment of o/w emulsions for industrial scale operation as well. However, the cost of these membranes is significantly higher (2000–4000 $/m^2 [13]) due to the higher cost of inorganic precursors such as alumina, zirconia and higher sintering temperature (more than 1100 °C) during membrane fabrication [14]. This is also due to the fact that higher sintering temperatures demand higher electrical energy and hence operating costs. In addition, higher sintering temperatures may also give rise to enhancement in furnace power specifications and hence the installed costs. Therefore, higher sintering temperatures translate to higher membrane fabrication costs. In other words, existing trends in industrial applications of membrane systems indicate the dominance of polymeric membranes over ceramic membranes. Thereby, the development of low-cost ceramic membranes (200–400 $/m^2) with longer life span is anticipated to drive the economic competitiveness of ceramic membranes in the industry.

Wastewater process streams consisting of oil concentration ranging 50– 200 mg/l are common in process industries and are very difficult to separate [9] due to the formation of highly stable emulsions. The feasibility of low-cost ceramic membranes for the microfiltration (MF) of o/w emulsions with low feed concentrations ranging from 50 to 200 mg/l has not been verified so far and is therefore the primary objective of this work. In our earlier publication [14] we have reported the preparation of kaolin based ceramic membrane using different low-cost inorganic precursors such as kaolin, quartz, calcium carbonate, sodium carbonate, boric acid and sodium metasilicate. During membrane preparation, sintering temperature was kept below 900 °C to minimize the cost of the fabrication process without affecting the membranes performance. The cost of the fabricated ceramic membranes was estimated to be 130 $/m^2 based on retail price of inorganic precursors. Subsequently, the membrane cost was assumed to be 400 $/m^2 including fabrication and module costs, which is significantly comparable to that of the conventional polymeric membranes (50–200 $/m^2) and far lower than other commercially available ceramic membranes (2000–4000 $/m^2). This work reports the application of the prepared low-cost ceramic membrane for the treatment of o/w emulsions using dead-end MF. The maximum feed-concentration of the o/w emulsions was taken as 150 mg/l to confine the study to the challenging task of separating highly stable emulsions. Permeate flux decline was analyzed using various flux decline models to get an insight into the nature of membrane fouling during filtration. Based on observed MF flux decline data, phenomenological models were proposed to illustrate the dependency of total hydraulic resistance of membrane on initial oil concentration (C), transmembrane pressure drop (ΔP) and filtration time (t).

2. Experimental

2.1. Ceramic membrane

Flat circular disk type ceramic microfiltration (MF) membrane of 5.25×10^{-2} m diameter and 4.5×10^{-3} m thickness was prepared from a clay mixture with the composition as kaolin (8 g), quartz (3 g), calcium carbonate (5 g), sodium carbonate (2 g), boric acid (1 g) and sodium metasilicate (1 g) by paste casting method. The hydraulic pore diameter and total porosity of the membrane was evaluated to be 0.77 μm and 42%, respectively. Detailed description of the preparation method, membrane characterizations and cost of the membrane are presented elsewhere [14]. A summary of the membrane properties is given in Table 1. Before MF experiment, two stage compaction experiments were performed. In the first stage, membrane was compacted at 310 kPa pressure for 180 min in the membrane cell. It was found that after 90 min of operation a constant

Table 1
Properties of used ceramic membrane

Properties	Value
Membrane permeable area (m^2)	1.66×10^{-3}
Thickness (m)	4.5×10^{-3}
Hydraulic pore diameter (μm)	0.77
Hydraulic permeability (m^3/m$^2 \cdot$ s $\cdot$ Pa)	1.94×10^{-9}
Intrinsic membrane resistance, R_m (m^2/m^3)	5.78×10^{11}
Total porosity	42%
Material cost ($/m^2)	130

flux (≈6.029 × 10^{-4} m^3/m^2 s) was observed, which indicated that the compaction was over. The membrane was dismantled and kept overnight. In the second stage, the compacted membrane was used again for the determination of pure water flux and found that the flux remains almost unchanged (~6.032 × 10^{-4} m^3/m^2 s) even after 180 min of operation. This confirms that no significant variation in membrane structure occurred after compaction.

2.2. Microfiltration of oil-in-water emulsions

Crude oil collected from Guwahati Refinery, Indian Oil Corporation Limited (IOCL), India, was used without any treatment to prepare synthetic o/w emulsions. Oil-in-water emulsions were prepared using distilled water and crude oil by placing the o/w mixture in a sonicator tank (Make: Elmasonic; Model: S30H) for 15 h at a temperature of 25 °C. Further details on the preparation of stable oil-in-water emulsions and their characterization techniques were summarized elsewhere [15]. Deadend MF experiments were carried out in a membrane permeation cell of capacity 125 ml in batch mode. Since dead-end MF enables the realization of severe fouling conditions, the performance of the membrane could be useful to evaluate general fouling tendency. The experimental setup (as shown in Fig. 1) consists of a Teflon tubular cell with a flat circular Teflon base plate which contains the membrane housing. The feed was filled in the tubular section from the top. The membrane was placed in a Teflon casing and sealed with epoxy resin and then placed in the membrane housing provided on the base plate. The cell was pressurized with compressed air. To carry out several experimental runs using the same membrane, membrane cleaning procedures were followed so as to regain their hydraulic permeability. Procedures adopted for membrane cleaning and subsequent permeability analysis have been elaborated elsewhere [9].

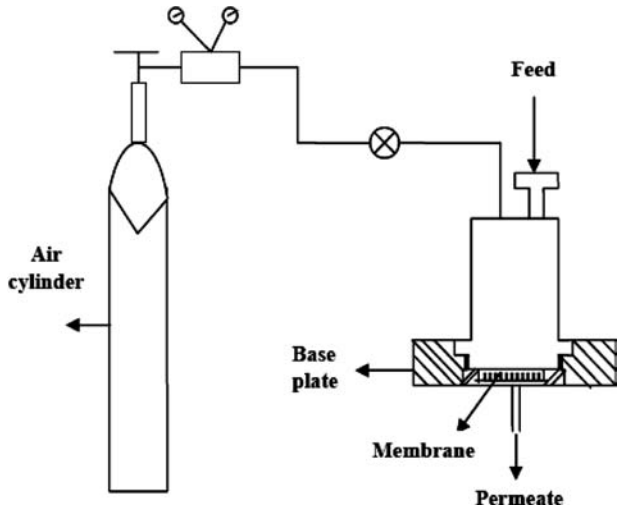

Fig. 1. Schematic of the experimental set-up.

2.3. Characterization techniques

Droplet size distribution in the prepared o/w emulsions were measured using a laser particle size analyzer (Make: Malvern; Model: Mastersizer 2000). Microfiltration experiments of the synthetic o/w emulsions were carried out with four different concentrations of oil (50, 75,100 and 150 mg/l) to observe the effect of oil concentration on the permeate flux and oil rejection efficiency of the membrane. Five transmembrane pressures differentials (ΔP) of 41.37, 82.74, 124.11, 165.47 and 206.84 kPa were used to observe the effect of ΔP on the permeate flux and oil rejection efficiency of the membrane. Permeate from the bottom of the cell was collected and its cumulative weight was measured with the help of an electronic balance. Permeate was collected at 5 min interval for the measurement of its oil concentration whereas flux data was taken in the interval of 1 min during the experiment. All experiments were conducted at room temperature (≈25 °C). The permeate flux (J) and the percent oil rejection (R) were calculated using the following equations:

$$J = \frac{V}{S \times \Delta t} \tag{1}$$

$$R = \left(1 - \frac{C_P}{C}\right) \times 100 \tag{2}$$

where V(m^3) is the volume of permeate, S (m^2) is the permeable area of the membrane, Δt(s) is the time, C_p and C are the oil concentration at permeate and feed. The oil concentrations in permeate and feed were determined using a UV–Vis spectrophotometer (Make: Perkin Elmer Precisel; Model: Lambda 35) by measuring absorbance at a wavelength of 235 nm where maximum absorbance was observed [9,15].

3. Theory of membrane fouling mechanism

Hermia [16] outlined four empirical models to represent dead-end MF membrane fouling mechanisms at constant pressure. These correspond to complete pore blocking, standard pore blocking, intermediate pore blocking and cake filtration. Fig. 2 shows the schematics of different membrane fouling mechanisms. The models were developed using constant pressure filtration law:

$$\frac{d^2t}{dV^2} = K\left(\frac{dt}{dV}\right)^n \tag{3}$$

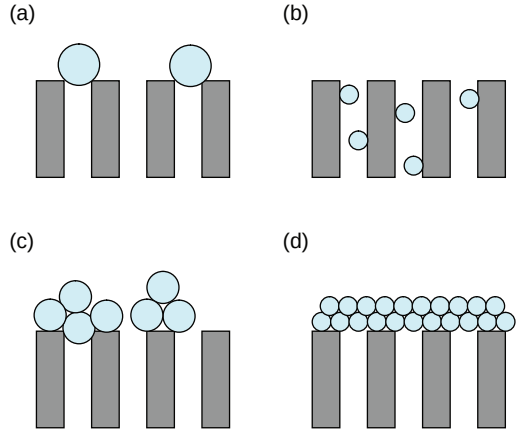

Fig. 2. Schematic representation of blocking mechanism (a) intermediate pore blocking, (b) complete pore blocking, (c) standard pore blocking and (d) cake filtration.

where selection of parameter n with values 2, 1.5, 1 and 0 corresponds to complete pore blocking, standard pore blocking, intermediate pore blocking and cake filtration, respectively. Corresponding modeling expressions for various fouling mechanisms representing time dependent flux are:

(a) $n = 2$: Complete pore blocking:

$$\ln\left(J^{-1}\right) = \ln\left(J_0{}^{-1}\right) + k_b t \tag{4}$$

(b) $n = 1.5$: Standard pore blocking:

$$J^{-0.5} = J_0{}^{-0.5} + k_s t \tag{5}$$

(c) $n = 1$: Intermediate pore blocking:

$$J^{-1} = J_0{}^{-1} + k_i t \tag{6}$$

(d) $n = 0$: Cake filtration:

$$J^{-2} = J_0{}^{-2} + k_c t \tag{7}$$

It can be further observed that a plot of $\ln(J^{-1})$ vs. t, $J^{-0.5}$ vs. t, J^{-1} vs. t and J^{-2} vs. t shall be a straight line with a slope of k_b, k_s, k_i and k_c and y-intercept of $\ln(J_0{}^{-1})$, $(J_0{}^{-0.5})$, $(J_0{}^{-1})$ and $(J_0{}^{-2})$ for complete pore blocking, standard pore blocking, intermediate pore blocking and cake filtration model, respectively. Also, parameters associated to these models subsequently have a physical relevance. The appropriate fitness and competence of various fouling models can be confirmed by comparing the values of coefficient of correlation (R^2) obtained from the linear regression analysis. A detailed description of the various pore blocking models has been presented elsewhere [17].

4. Results and discussion

4.1. Emulsion droplet size distribution

Fig. 3 shows the droplet size distribution of emulsion with initial feed oil concentration. As indicated by the profile, a bimodal distribution of the oil droplet curve was apparent for all four emulsions studied in this work. The droplet size of the emulsion varied between 0.04 and 100 μm, with more than 96% of the oil droplets possessing sizes between 0.04 and 10 μm. Further, it can also be observed that the volume percent of emulsions with smaller droplet sizes (0.1 μm) increased with an increase in the oil concentration. However, with an increase in oil concentration, the volume percent of the bigger oil droplets (10–100 μm) increased, which eventually contributed to the overall increase in the average droplet size. However, the droplet volume distribution amongst these droplets is insignificant to visualize in the graph presented in Fig. 3. A similar observation was found for the enhancement of average oil droplet size with increasing concentration in the literature [18] for oil–wastewater systems. The average droplet sizes of the emulsions were 0.56, 0.75, 0.78 and 0.85 μm for emulsions prepared with 50, 75, 100 and 150 mg/l oil concentration, respectively.

4.2. Effect of transmembrane pressure and feed concentration on permeate flux

Permeate flux profiles with respect to time for different initial feed oil concentrations (50–150 mg/l) and transmembrane pressure drops (41.37, 82.74, 124.11, 165.47 and 206.84 kPa) are illustrated in Fig. 4a–d. These figures depict that a sharp decline in permeate flux existed within the initial 5–10 min of experimental run. For instance, for a feed oil concentration of 100 mg/l

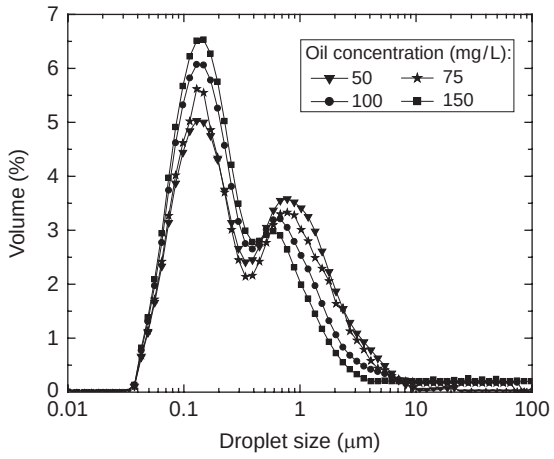

Fig. 3. Droplet size distribution of oil-in-water emulsion varying oil concentration.

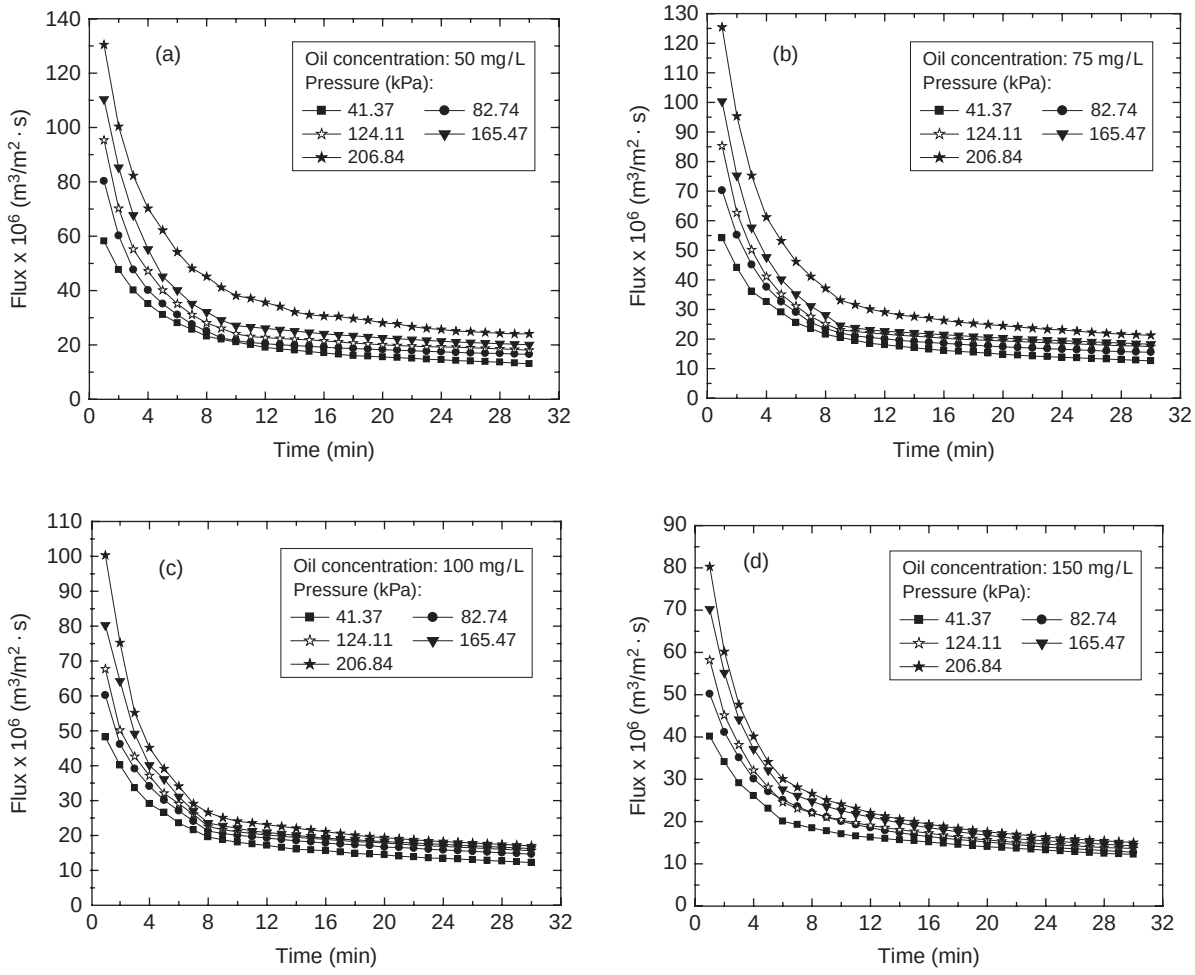

Fig. 4. Variation of permeate flux with time at different transmembrane pressure for different initial oil concentration: (a) 50 mg/l, (b) 75 mg/l, (c) 100 mg/l, (d) 150 mg/l.

and transmembrane pressure drop of 41.37 kPa, the permeate flux reduced from 48.16×10^{-6} to 18.06 m^3/m^2 s within the first 10 min of permeation and eventually reached a value of 12.24×10^{-6} m^3/m^2 s after 30 min of experimental run (Fig. 4c). The transitional time dependent flux decline was due to the combined effect of pore blocking of ceramic porous structure and formation of thin oily film layer over the membrane surface. Also, it is observed that the permeate flux increases with an increase in transmembrane pressure. For an oil concentration of 100 mg/l, the initial permeate flux increased from 48.16×10^{-6} to 100.34×10^{-6} m^3/m^2 s when ΔP was increased from 41.37 to 206.84 kPa. These observed trends were due to the reason that at higher feed concentrations, higher quantities of oil droplets deposit over the membrane surface and create a thick oily film to enhance membrane fouling.

The observed permeate flux data for the prepared ceramic membrane was comparable with the flux data reported for polymeric and ceramic membranes in the literature [19]. While the prepared ceramic membrane provided a terminal flux of 13.64×10^{-6} m^3/m^2 s at 150 mg/l feed oil concentration and transmembrane pressure differential of 124.11 kPa, Millipore 0.45 mm (hydrophilic PVDF), Gelman 0.1 μm (hydrophilic polysulphone), Ceramesh 0.1 μm (hydrophilic zirconia coated, nickel alloy mesh composite membrane) membranes provided 0.11×10^{-6}, 4.36×10^{-6}, 2.86×10^{-6} and 1.77×10^{-6} m^3/m^2 s, respectively at an ΔP of 120 kPa and feed oil concentration of 500 mg/l.

4.3. Effect of transmembrane pressure and feed concentration on oil rejection

The variation of percent crude oil rejection with time at five different transmembrane pressure differentials and feed oil concentrations is presented in Fig. 5a–d. In general, it was observed that the membrane rejection

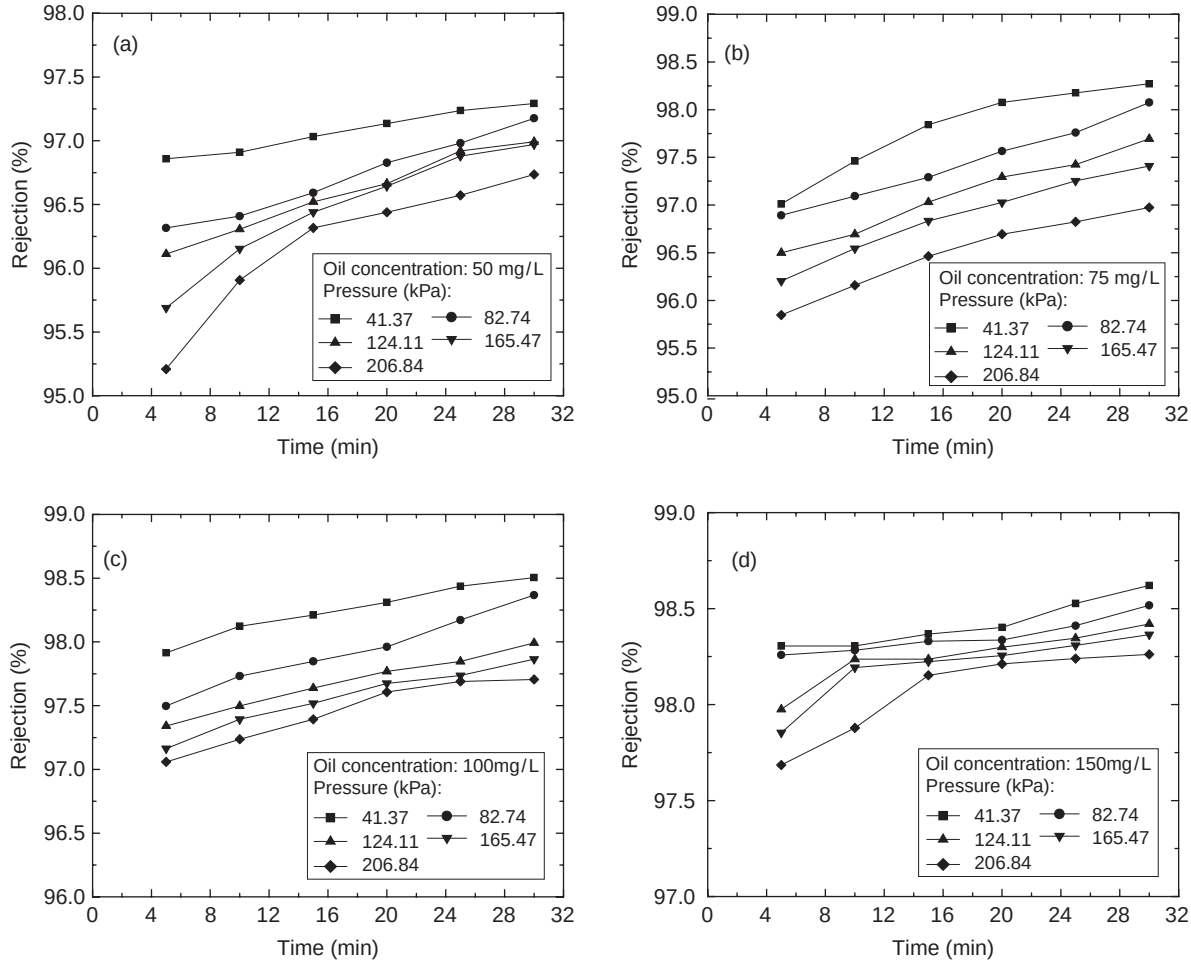

Fig. 5. Variation of oil rejection with time at different transmembrane pressure for different initial oil concentration: (a) 50 mg/l, (b) 75 mg/l, (c) 100 mg/l, (d) 150 mg/l.

efficiency slightly increased with time. At 100 mg/l feed oil concentration (Fig. 5c), the oil rejection efficiency increased from 97.9% (5 min) to 98.5% (30 min). The possibility of slight enhancement in rejection efficiency is due to the gradual reduction in the membrane pore diameter due to the adsorption of the oil droplets in the membrane pores. Also, an increase in pressure enabled a reduction in rejection efficiency. At 50 mg/l feed oil concentration, with an increase in ΔP from 41.37 to 206.84 kPa, the oil rejection efficiency reduced from 97.29% to 96.74%. Similar trends were also observed at the other three feed oil concentrations (50, 75 and 150 mg/l). These observed trends in rejection efficiency agree well with the data reported for ZrO_2 membranes in the literature [11]. With an increase in ΔP, wetting and coalescence of oil droplets enhances. Due to this reason, some oil droplets pass through the membrane pores at higher driving force and reach the permeate stream. Also, the membrane oil rejection efficiency reduced with a reduction in feed oil concentration with the maximum rejection of 98.62% observed at 150 mg/l feed concentration and ΔP of 41.37 kPa. This was due to the creation of comparatively thin oily layer (as less oil droplets are present) over the membrane surface at lower feed oil concentrations and thicker oily layer at higher oil concentrations.

4.4. Identification of competent flux decline mechanism

The identification of competent flux decline mechanism is very important for any MF processes as the pertinent fouling mechanism that best represents the experimental data trends indicates upon the reversibility and irreversibility of the fouling. The decline in permeate flux during dead-end MF of o/w emulsions has been analyzed using different membrane pore blocking models as discussed in Section 3. To find the most prominent fouling mechanism among the pore blocking models, linear plots corresponding to Eqs. (4)–(7) were prepared.

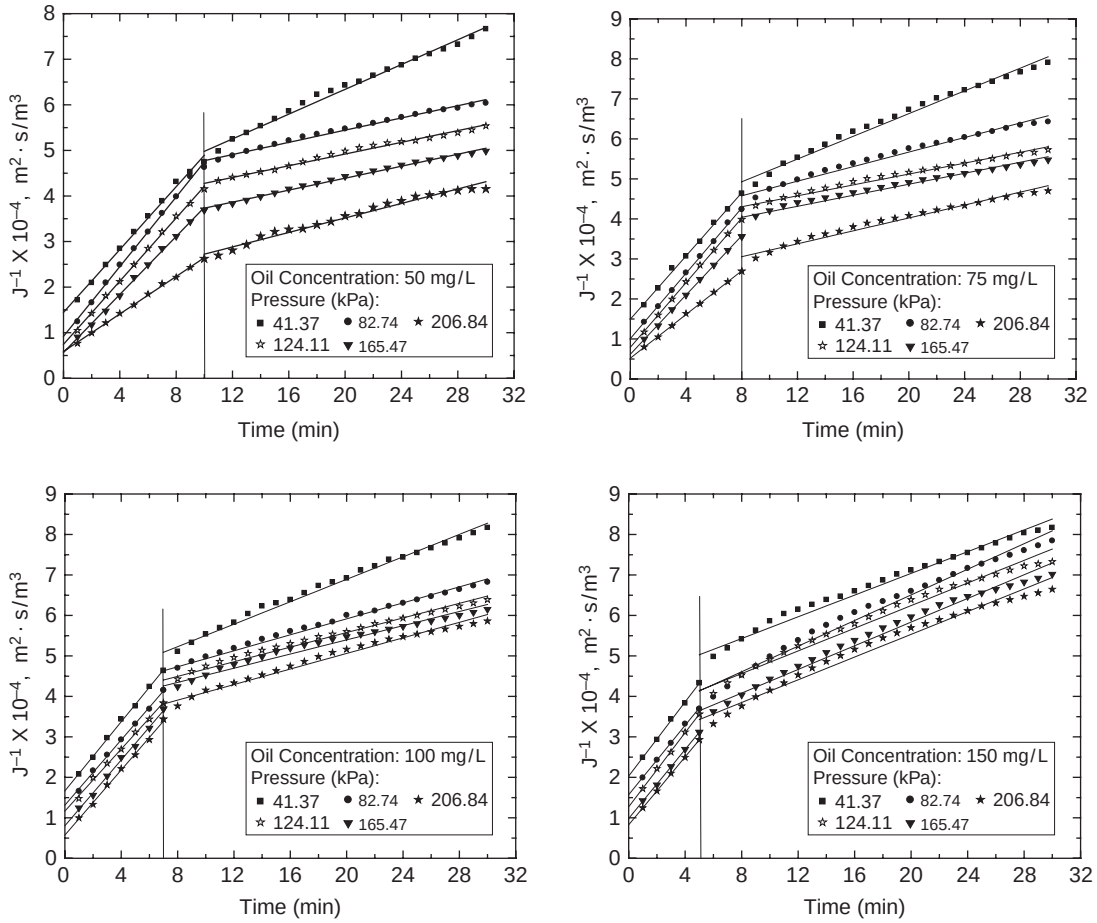

Fig. 6. Linear plot of permeate flux vs. time for intermediate pore blocking model for different initial oil concentration: (a) 50 mg/l, (b) 75 mg/l, (c) 100 mg/l, (d) 150 mg/l.

Figs. 6 and 7 illustrate the fitness of intermediate pore blocking model and cake filtration model for all the oil concentrations, respectively. Similar types of plots were obtained for standard pore blocking and complete pore blocking whose figures were not shown. From all these figures, it was observed that the experimental data sets followed two hierarchical linear flux trends that correspond to initial regime of 5–10 min and the later regime up to 30 min. From the figure it was observed that the time durations for initial regimes were 10, 8, 7 and 5 min for initial oil concentration of 50, 75, 100 and 150 mg/l, respectively. A reduction in initial time regime with an increase in oil concentration was due to the presence of higher amount of oil droplets which enables pore blocking at lesser time. Possibly, the data also infers that the pertinent flux decline adopted two different pore blocking mechanisms. This observation was in agreement with the flux decline trends presented during MF of oily wastewater with a polymeric membrane [20].

Eventually, the experimental flux data was further analyzed separately in these two time regimes, namely the initial regime corresponding to the first 5–10 min of MF and the later regime so as to identify the most competent combinations of various models in both the regimes. In order to visualize the most competent fouling phenomena during the initial phases, linear regression analysis including slope, intercept as well as correlation coefficients (R^2) for all permeate flux data were calculated. To find the most appropriate fouling mechanism, the correlation coefficients (R^2) were compared initially. Table 2 summarized the calculated values of correlation coefficients (R^2) for all models in both regimes. For the initial regime (up to 5–10 min), it can be critically observed from Fig. 7 that there exists negative intercept for cake filtration model. As negative intercept values signifies an infeasible negative initial permeate flux, this model is ignored in the subsequent analysis of flux decline for the initial regime. Further, it can be also observed in Table 2 for the same regime that R^2 values for all other models (standard pore blocking, complete pore blocking and intermediate pore blocking) is in comparatively acceptable range (0.95–0.99).

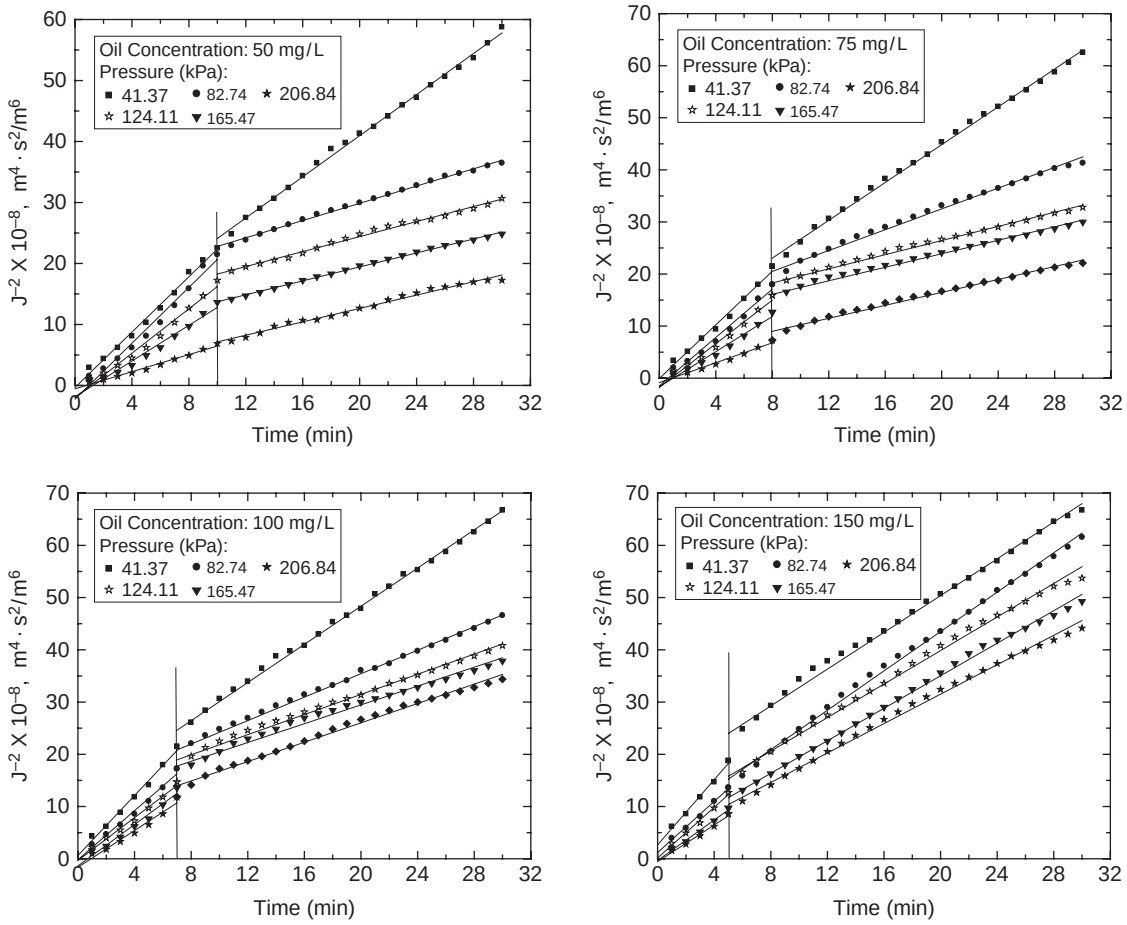

Fig. 7. Linear plot of permeate flux vs. time for cake filtration model for different initial oil concentration: (a) 50 mg/l, (b) 75 mg/l, (c) 100 mg/l, (d) 150 mg/l.

To further analyze the applicability of various models, percent error of experimental and predicted permeate flux using slope and intercept values for those models were evaluated using the following expression for analysis:

$$Error(\%) = \left(\frac{J_{\text{Experimental}} - J_{\text{Calculated}}}{J_{\text{Experimental}}} \right) \times 100 \qquad (8)$$

Fig. 8a shows the results obtained from error analysis for the experimental condition of 150 mg/l initial oil concentration and 41.37 kPa transmembrane pressure drop. Based on the observations from Fig. 8a, it can be inferred that intermediate pore blocking model is the most appropriate model to account for the flux decline mechanism during the initial regime with the lowest errors. Similar trends were also observed for other experimental conditions as well.

Also, for the later regime, correlation coefficients (R^2) and error analysis were evaluated for all the models. Based on observed values of R^2 in Table 2, it can be inferred that all the four models indicated good fitness ($R^2 > 0.99$). Fig. 8b shows the result obtained from error analysis for experimental condition of 75 mg/l initial oil concentration and 124.11 kPa transmembrane pressure drop. Based on the observations from Fig. 8b, it can be inferred that the errors were minimum for cake filtration model. Hence the cake filtration model was selected as the most appropriate to represent the flux decline during the later regime with lowest error. In summary, it can be concluded that intermediate pore blocking followed with cake filtration represent the most competent combination of fouling mechanisms for the observed membrane flux decline.

Table 3 summarizes the final values of slope and intercept for both regimes. Based on these values, predicted flux was evaluated and compared with the experimental values to evaluate the errors. Table 4 summarized the values of maximum and average errors for all the data sets. Fig. 8c presents a parity plot between experimental and evaluated flux using the best combinations of models

Table 2
Observed values of correlation coefficient (R^2) obtained by linear regression analysis of permeate flux data for different membrane pore blocking models (Eqs. (7 – 10))

Concentration of oil (mg/l)	Pressure (kPa)	Complete pore blocking		Standard pore blocking		Intermediate pore blocking		Cake filtration	
		Initial regime	Final regime	Initial regime	Final regime	Initial regime	Final regime	Initial regime	Final regime
50	41.37	0.963	0.972	0.984	0.982	0.995	0.989	0.992	0.997
	82.74	0.955	0.978	0.985	0.983	0.998	0.987	0.981	0.994
	124.11	0.954	0.977	0.986	0.982	0.999	0.986	0.981	0.991
	165.47	0.960	0.987	0.988	0.991	0.998	0.994	0.977	0.998
	206.84	0.962	0.962	0.988	0.972	0.999	0.989	0.983	0.989
75	41.37	0.974	0.964	0.991	0.976	0.998	0.986	0.988	0.997
	82.74	0.975	0.950	0.993	0.962	0.999	0.973	0.981	0.994
	124.11	0.964	0.982	0.989	0.987	0.999	0.991	0.982	0.996
	165.47	0.967	0.982	0.991	0.987	1.000	0.991	0.978	0.996
	206.84	0.970	0.962	0.992	0.973	1.000	0.982	0.978	0.994
100	41.37	0.981	0.959	0.993	0.973	0.998	0.984	0.990	0.996
	82.74	0.974	0.946	0.991	0.961	0.998	0.973	0.986	0.999
	124.11	0.966	0.914	0.987	0.935	0.997	0.993	0.989	0.998
	165.47	0.978	0.963	0.993	0.972	0.997	0.980	0.971	0.991
	206.84	0.970	0.967	0.992	0.976	0.998	0.984	0.967	0.994
150	41.37	0.993	0.968	0.997	0.979	0.999	0.988	0.992	0.997
	82.74	0.989	0.950	0.996	0.968	0.999	0.982	0.994	0.998
	124.11	0.986	0.958	0.996	0.972	0.999	0.983	0.989	0.996
	165.47	0.989	0.959	0.997	0.974	1.000	0.985	0.987	0.997
	206.84	0.984	0.944	0.996	0.963	1.000	0.978	0.985	0.996

in both the regimes. As shown, a good fitness between experimental and evaluated values is observed and henceforth, the suggested model combination is applicable for the analysis, design, planning and scheduling of time dependent MF processes for oil-water emulsion separation in the process industries.

Fig. 9 shows the variation of transition time from initial regime (intermediate pore blocking) to later regime (cake filtration) with varying oil concentration. From the figure it can be observed that with an increase in feed oil concentration transition time period decreases. Also, linear extrapolation of the data trends reveals that for feed oil concentrations above 250 mg/l, only cake filtration would be the flux decline mechanism.

4.5. Phenomenological modeling

From pore blocking model analysis it was observed that flux decline was due to the pore blocking and cake filtration. Due to pore blocking and cake filtration total permeate flux declined continuously. This decline also can be expressed as an increase in total membrane resistance with time (R_t). The variation of R_t with time is dependent on ΔP and feed oil concentration C. Therefore, phenomenologically $R_t(t)$ can be expressed as a function of dependent variables like time (t), ΔP, C as:

$$R_t(t) = \frac{\Delta P}{\mu_P J_J(t)} = f(t, \Delta p, C) \tag{9}$$

In the above expression, the fitness of the most appropriate nonlinear functions for time (t), ΔP and C was determined from the nonlinear regression analysis of the experimental data using genetic algorithm. The experimental data points were attempted to fit various nonlinear modeling expressions such as power, exponential and logarithmic models, etc. on a trial and error basis to obtain the appropriate nonlinear model and its parameters that offers minimum errors with respect to the experimental R_t values. From the analysis, $R_t(t)$ was found to adopt the following empirical correlation at constant ΔP adopting the power law model:

$$R_t = A \times (C)^a \left(\frac{t}{60}\right)^b \tag{10}$$

For constant feed oil concentration, $R_t(t)$ was found to adopt the following empirical correlation

$$R_t = D \times (\Delta P)^d \times \left(\frac{t}{60}\right)^e \tag{11}$$

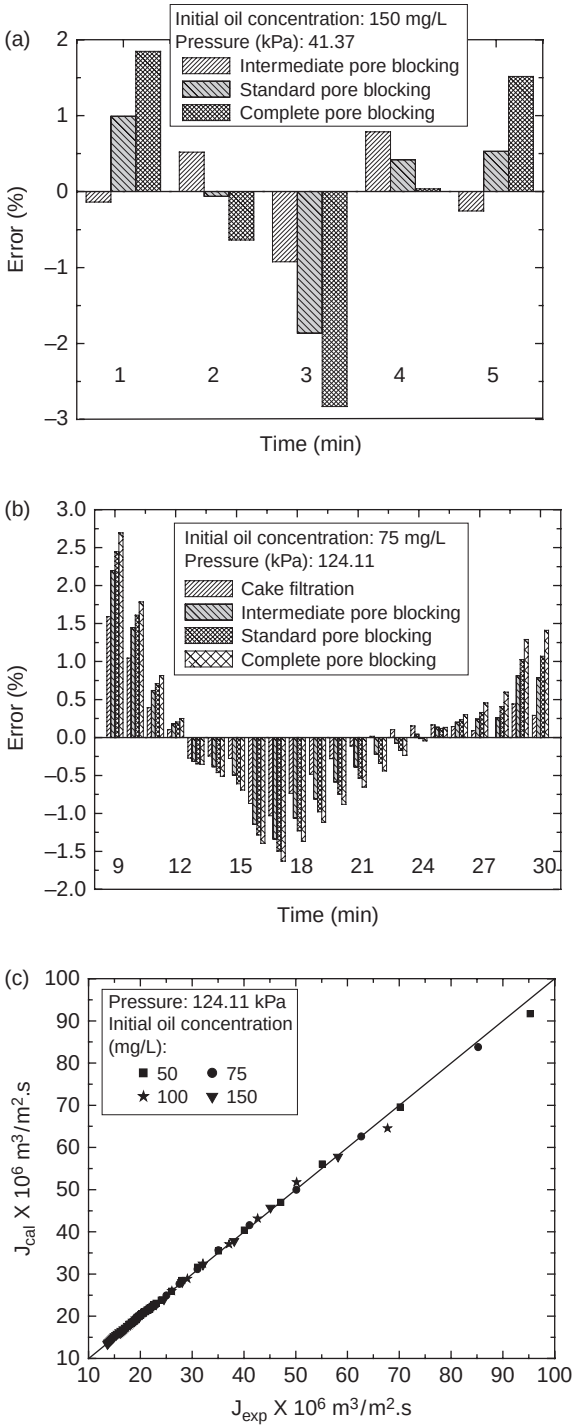

Fig. 8. (a) Variation of error (%) with time for the initial regime. Initial oil concentration: 150 mg/l and transmembrane pressure: 41.37 kPa. (b) Variation of error (%) with time for the initial regime. Initial oil concentration: 75 mg/l and transmembrane pressure: 124.11 kPa. (c) Parity plot of experimental and calculated permeate flux using combination of intermediate pore blocking and cake filtration model.

Table 3
Observed values of slope and intercept obtained by linear regression analysis of permeate flux data for initial (intermediate pore blocking) and final regime (cake filtration)

Concentration of oil (mg/l)	Pressure (kPa)	Initial regime (Intermediate pore blocking)		Final regime (Cake filtration)	
		(J_o^{-1})	(k_i)	$(J_o^{-2})\times 10^{-7}$	$(k_c)\times 10^{-7}$
50	41.37	14458	3446.5	72.39	16.85
	82.74	9204	3824	157.27	7.07
	124.11	7447	3465	121.15	6.15
	165.47	5667	3181	79.95	5.72
	206.84	5888	2057	16.65	5.48
75	41.37	1492	3952	89.87	17.95
	82.74	1009	4081	132.78	9.66
	124.11	7905	4039	135.56	6.48
	165.47	6174	3703	119.44	6.04
	206.84	5185	2731	45.44	5.99
100	41.37	16650	4272	126.53	17.90
	82.74	13128	4032	139.41	10.80
	124.11	11666	3831	133.27	9.14
	165.47	8024	4067	125.60	8.52
	206.84	5725	4024	80.59	9.02
150	41.37	20296	4585	163.22	17.08
	82.74	15708	4287	61.59	18.69
	124.11	12714	4582	84.46	15.74
	165.47	9829	4263	43.50	15.36
	206.84	8251	4202	37.27	13.91

Table 4
Summary of calculated values of errors

Concentration of oil (mg/l)	Pressure (kPa)	Maximum error (%)	Average error (%)
50	41.37	4.03	0.90
	82.74	4.38	0.74
	124.11	3.86	0.79
	165.47	2.93	0.78
	206.84	3.50	1.23
75	41.37	3.39	0.77
	82.74	2.33	0.71
	124.11	1.83	0.49
	165.47	2.42	0.47
	206.84	2.64	0.92
100	41.37	1.86	0.61
	82.74	3.20	0.71
	124.11	4.72	0.95
	165.47	3.62	1.30
	206.84	3.52	1.10
150	41.37	2.78	0.74
	82.74	3.64	0.80
	124.11	2.45	0.79
	165.47	1.48	0.60
	206.84	3.24	0.97

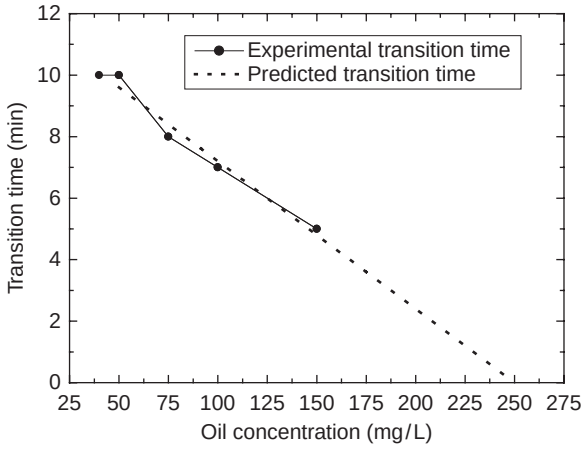

Fig. 9. Variation of transition time with feed oil concentration during MF of oil-in-water emulsions.

Tables 5a and 5b presents a summary of values of regression parameters (A, a, b, D, d, e) obtained from the nonlinear regression analysis. From the tables it can be observed that the average errors for all the cases were less than 4.59% with a maximum error of 8.73%. However for design purpose, a better solution will be combination of both pressure and oil concentration. In that case $R_t(t)$ was found to adopt the following empirical correlation as

$$R_t = M \times (\Delta P)^m \times (C)^q \times \left(\frac{t}{60}\right)^r \quad (12)$$

Table 5a
Calculated values of various regression parameters (A, a and b) corresponding to Eq. (10)

Pressure (kPa)	$A \times 10^{-10}$	a	b	Average error (%)	Maximum error (%)
41.37	43.457	0.145	0.451	3.88	5.34
82.74	52.120	0.223	0.452	3.78	7.07
124.11	46.459	0.309	0.469	4.42	8.73
165.47	44.200	0.359	0.485	4.40	6.29
206.84	38.611	0.428	0.471	4.59	7.52

Table 5b
Calculated values of various regression parameters (D, d and e) corresponding to Eq. (11)

Concentration of oil (mg/L)	$D \times 10^{-10}$	d	e	Average error (%)	Maximum error (%)
50	6.105	0.651	0.505	3.46	5.88
75	5.448	0.710	0.476	4.37	6.84
100	4.397	0.803	0.438	3.44	5.41
150	4.239	0.830	0.439	2.85	5.78

Table 5c
Calculated values of various regression parameters (M, m, q and r) corresponding to Eq. (12)

$M \times 10^{-10}$	m	q	r	Average error (%)	Maximum error (%)
1.327	0.749	0.295	0.465	6.13	9.48

A summary of regression parameters M, m, q and r have been shown in Table 5c. Fig. 10 present the variation of calculated and experimentally obtained R_t values using Eq. (12). From the figures it can be observed that the fitness of the calculated values of R_t with the experimental observed R_t was in acceptable range for all values of ΔP and C. The average error and maximum error were calculated as 6.13% and 9.48%, respectively. This indicates that the fouling of the membrane follows a power-law trend with an increase in ΔP and C. The fitness of power-law models to represent phenomenologically the pertinent flux decline infer that a moderate hydraulic resistance growth with time exists for the chosen feed oil concentrations and operational transmembrane pressure differentials. An increase in R_t with an increase in both ΔP and C was due to the higher adsorption of oil droplets at higher combinations of transmembrane pressure differentials and oil concentrations as presented in Section 4.3.

5. Conclusion

This work demonstrated the application of cost-effective kaolin based inorganic membranes for the treatment of o/w emulsions. Microfiltration experiments using prepared ceramic membrane was conducted in batch mode of operation with synthetic o/w emulsions of various feed concentrations ranging from 50 to 160 mg/l. The membrane exhibited 93.81% to 98.51% oil rejection efficiency with a permeate flux of 10.54×10^{-6} m^3/m^2 s to 22.1×10^{-6} m^3/m^2 s at various values of ΔP ranging from 41.37 to 206.8 kPa after 30 min of experimental run. The decline in permeate flux has been analyzed using different pore blocking models. The reduction in permeate flux was initially (first 5 to 10 min depending on oil concentration) due to intermediate pore blocking and later due to cake filtration. Phenomenological models were also proposed to illustrate the dependency of total hydraulic resistance of membrane on C, ΔP and time (t). Finally, based on the experimental and theoretical analysis, it can be concluded that kaolin based low-cost inorganic membranes are very promising for the treatment of industrial low concentration range o/w emulsions and could meet the technical challenges posed by tighter environmental legislations, within an affordable process cost.

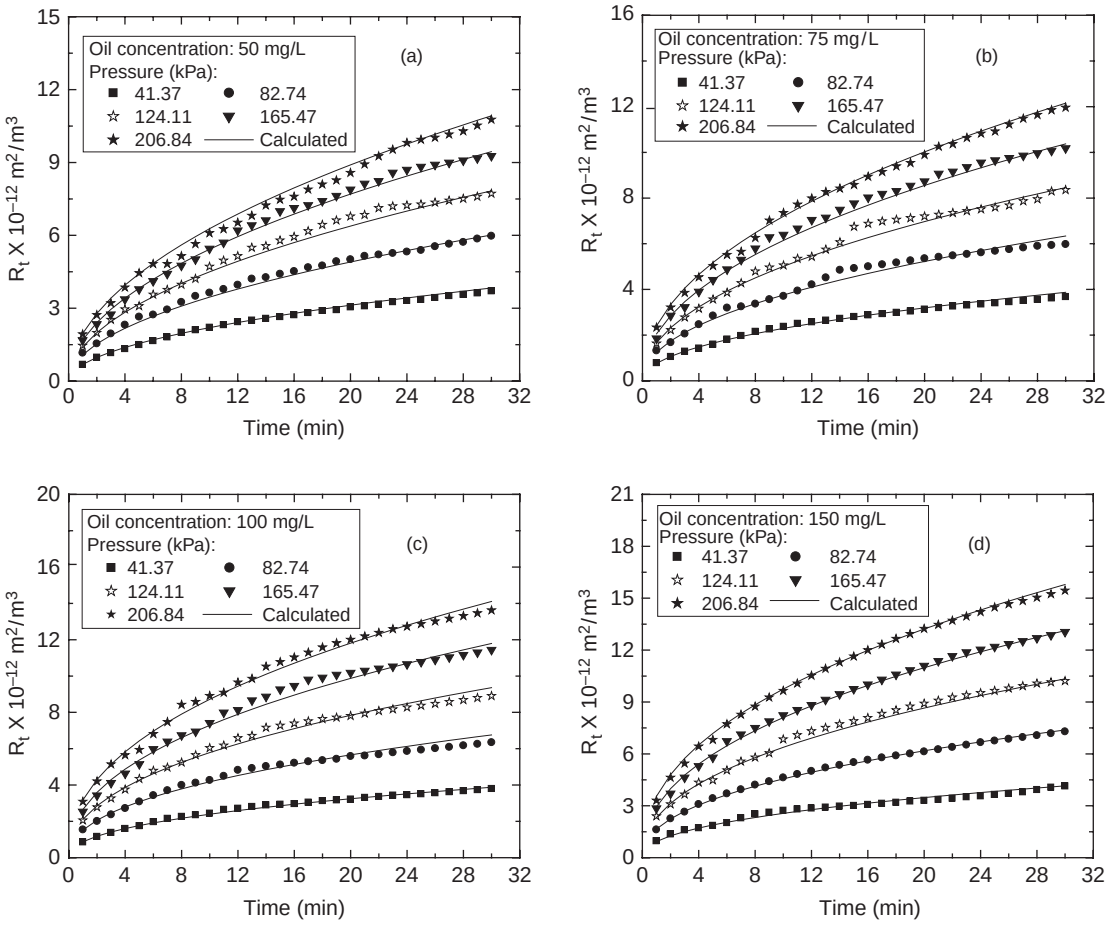

Fig. 10. Experimental and calculated values of total membrane resistance with time at different trans-membrane pressure for various initial oil concentrations: (a) 50 mg/l, (b) 75 mg/l, (c) 100 mg/l, (d) 150 mg/l.

Symbols

- A — Constant in Eq. (10)
- a — Constant in Eq. (10)
- b — Constant in Eq. (10)
- D — Constant in Eq. (11)
- d — Constant in Eq. (11)
- e — Constant in Eq. (11)
- J — Permeate flux (m^3/m^2 s)
- J_0 — Initial permeate flux (m^3/m^2 s)
- K — Constant in Eq. (2) (units depend on the parameter n)
- k_b — Complete blocking model constant (Eq. (3)) (s^{-1})
- k_c — Cake filtration model constant (Eq. (6)) (s/m^2)
- k_i — Intermediate pore blocking model constant (Eq. (5)) (m^{-1})
- k_s — Standard pore blocking model constant (Eq. (4)) ($m^{-0.5}$ $s^{-0.5}$)
- M — Constant in Eq. (12)
- m — Constant in Eq. (12)
- n — Constant in Eq. (2) that depends on the fouling mechanism (dimensionless)
- ΔP — Trans-membrane pressure (kPa)
- Q — Volume of permeate (m^3)
- q — Constant in Eq. (12)
- R^2 — Square of correlation coefficient (dimensionless)
- r — Constant in Eq. (12)
- S — Permeable area of membrane (m^2)
- t — Sampling time (s)
- V — Cumulative volume of permeate (m^3)
- μ_p — Viscosity of permeate (kPa.s)

References

[1] A. Bevis, The treatment of oily water by coalescing, Filtr. Sep., (1992) 295–301.
[2] C. Ratlege, Mini review compilation biodegradation and biotransformations of oils and fats, J. Chem. Tech. Biotechnol., 55 (1992) 397–414.

[3] R.M. Bande, B. Prasad, I.M. Mishra and K.L. Wasewar, Oil field effluent water treatment for safe disposal by electroflotation, Chem. Eng. J., 137 (2008) 503–509.
[4] A.Y. Hosny, Separating oil from oil-water emulsions by electroflotation technique, Sep. Technol., 6 (1996) 9–17.
[5] A.L. Ahmad, S. Sumathi and B.H. Hameed, Coagulation of residue oil and suspended solid in palm oil mill effluent by chitosan, alum and PAC, Chem. Eng. J., 118 (2006) 99–105.
[6] A.E.Kayar, M. Hussein, A.A. Zatout, A.Y. Hosny and A.A. Amer, Removal of oil from stable oil–water emulsion by induced air flotation technique, Sep. Technol., 3(1993) 25–31.
[7] J.M. Benito, G. Rios, E. Ortea, E. Fernandez, A. Cambiella, C. Pazos and J. Coca, Design and construction of a modular pilot plant for the treatment of oil-containing waste waters, Desalination,147 (2002) 5–10.
[8] A. Salahi, T. Mohammadi, A.R. Pourb and F. Rekabdar, Oily wastewater treatment using ultrafiltration, Desalin. Water Treat., 6 (2009) 289–298.
[9] B. Chakrabarty, A.K. Ghoshal and M.K. Purkait, Ultrafiltration of stable oil-in-water emulsion by polysulfone membrane, J. Membr. Sci., 325 (2008) 427–437.
[10] M. Hesampoura, B. Simonb and M. Nyström, Ultrafiltration of oily water under different conditions, considering critical and limiting flux, Desalin. Water Treat., 9 (2009) 119–125.
[11] G.N. Vataia, D.M. Krsti b, A.K. Korisa, I.L. Gáspára and M.N. Teki c, Ultrafiltration of oil-in-water emulsion: Comparison of ceramic and polymeric membranes, Desalinat. Water Treat.., 3 (2009) 162–168.
[12] M. Cheryan, Ultrafiltration and Microfiltration Handbook. Techno. Pub. Co. Inc., 1998.
[13] S. Tennison, Current hurdles in the commercial development of inorganic membrane reactors, Membr. Technol., 2000 (128).
[14] B.K. Nandi, R. Uppaluri and M.K. Purkait, Preparation and characterization of low cost ceramic membranes for microfiltration applications, Appl. Clay Sci., 42 (2008) 102–110.
[15] B.K. Nandi, R. Uppaluri and M.K. Purkait, Treatment of oily waste water using low-cost ceramic membrane: Flux decline mechanism and economic feasibility, Sep. Sci Technol., 44 (2009) 2840–2869.
[16] J. Hermia, Constant pressure blocking filtration laws-application to power-law non-newtonian fluids, Trans. Inst. Chem. Eng. 60 (1982) 183–187.
[17] B.K. Nandi, B. Das, R. Uppaluri and M.K. Purkait, Microfiltration of mosambi juice using jow cost ceramic membrane, J. Food Eng., 95 (2009) 597–605.
[18] P. Lipp, C.H. Lee, A.G. Fane and C.J.D. Fell, A fundamental study of the ultrafiltration of oil–water emulsions, J. Membr. Sci., 36 (1988) 161–177.
[19] T.C. Arnot, R.W. Field and A.B. Koltuniewicz, Cross-flow and dead-end microfiltration of oily-water emulsions. Part II. Mechanisms and modelling of flux decline, J. Membr. Sci., 169 (2000) 1–15.
[20] B. Hu and K. Scott, Microfiltration of water in oil emulsions and evaluation of fouling mechanism, Chem. Eng. J., 136 (2008) 210–220.